Monthly Notices
of the
ROYAL ASTRONOMICAL SOCIETY

Mon. Not. R. Astron. Soc. **412,** 875–882 (2011) doi:10.1111/j.1365-2966.2010.17944.x

A new frequency–luminosity relation for long gamma-ray bursts?

T. N. Ukwatta,[1,2]★ K. S. Dhuga,[1] D. C. Morris,[1,2] G. MacLachlan,[1] W. C. Parke,[1] L. C. Maximon,[1] A. Eskandarian,[1] N. Gehrels,[2] J. P. Norris[3] and A. Shenoy[1]

[1]*Department of Physics, The George Washington University, Washington, DC 20052, USA*
[2]*NASA Goddard Space Flight Center, Greenbelt, MD 20771, USA*
[3]*Department of Physics and Astronomy, University of Denver, 2112 East Wesley Ave. Room 211, Denver, CO 80208, USA*

Accepted 2010 October 28. Received 2010 October 7; in original form 2010 July 12

ABSTRACT

We have studied power density spectra (PDS) of 206 long gamma-ray bursts. We fitted the PDS with a simple power law and extracted the exponent of the power law (α) and the noise-crossing threshold frequency ($f_{\rm th}$). We find that the distribution of the extracted α peaks around -1.4 and that of $f_{\rm th}$ around 1 Hz. In addition, based on a subset of 58 bursts with known redshifts, we show that the redshift-corrected threshold frequency is positively correlated with the isotropic peak luminosity. The correlation coefficient is 0.57 ± 0.03.

Key words: gamma-ray burst: general.

1 INTRODUCTION

Gamma-ray bursts (GRBs) show very complicated time profiles and, despite extensive investigations, are still not fully understood. The Fourier power density spectrum (PDS) of GRBs, on the other hand, seems to show relatively simple behaviour. Giblin, Kouveliotou & van Paradijs (1998) found that a typical PDS shows a low-frequency power-law component and a high-frequency flat component (usually associated with Poisson noise). Beloborodov, Stern & Svensson (1998, 2000) considered each GRB as a realization of some common stochastic process and showed that when averaged over many bursts the resulting PDS exhibits a power-law behaviour with an exponent of -1.67, which the authors note is consistent with the $-5/3$ Kolmogorov spectral index expected from processes involving turbulent flow. In addition, they claim that there is a break in the averaged PDS at $\sim$1 Hz. The authors were not in a position to correct their sample for the time dilation due to the cosmological redshifts.

Lazzati (2002) analysed GRB power spectra by dividing them into six luminosity bins using the variability–luminosity correlation (Fenimore & Ramirez-Ruiz 2000; Reichart et al. 2001; Guidorzi 2005; Guidorzi et al. 2005, 2006; Li & Paczyński 2006; Rizzuto et al. 2007). The PDS was averaged in each bin after correcting for pseudo-redshifts obtained through the variability–luminosity relation (Fenimore & Ramirez-Ruiz 2000). Lazzati (2002) showed that the dominant frequency ($f_{\rm d}$) of the PDS is strongly correlated with the variability parameter obtained by taking a modified variance of the detrended light curve (LC; Fenimore & Ramirez-Ruiz 2000). Here $f_{\rm d}$ is obtained by finding the maximum of the function $f \times$ PDS (f) (see Lazzati 2002 for more details). The author further states that the red-noise component of the averaged PDS for the six luminosity bins is well described by a broken power-law function with a low-frequency slope of $-2/3$ and a high-frequency slope of -2. In this case, the break frequency is a function of both luminosity and the variability parameter.

Borgonovo et al. (2007) did a similar analysis of power spectra but used measured redshift information to correct for time dilation effects before averaging. The burst sample was subdivided into two populations based on the calculated values of the autocorrelation function. After averaging, the PDS of one population shows a power-law index of ~ -2.0 (consistent with the spectral index expected of Brownian motion) and the PDS of the other population is characterized by a low-frequency exponentially decaying component and a high-frequency power-law component with an index of ~ -1.6 (which again is consistent with the $-5/3$ Kolmogorov spectral index).

Most of the previous work on PDS of GRBs has been based on observations with the Burst and Transient Source Experiment (BATSE) on the Compton Gamma Ray Observatory (Beloborodov et al. 1998, 2000; Giblin et al. 1998; Lazzati 2002; Borgonovo et al. 2007) where a relatively modest amount of redshift information is available. The launch of the *Swift* satellite (Gehrels et al. 2004) ushered in a new era of GRB research. Due to its rapidly disseminated, arcsecond GRB positions, *Swift* has enabled more subsequent redshift measurements of GRBs than ever before. The availability of redshift information enables the study of rest-frame properties of bursts and provides an opportunity for further exploration of correlations involving burst parameters such as luminosity and variability.

In this paper, we present a study of Fourier PDS of 206 *Swift* long bursts. Unlike previous work, we avoid averaging PDS of multiple bursts and examine them individually. We have developed a method to estimate the uncertainties in PDS for each burst. Then we extract PDS for all the GRBs in the sample and investigate the distribution of the extracted parameters. The structure of the paper is as follows.

★E-mail: tilan.ukwatta@gmail.com

In Section 2, we discuss our methodology for extracting the PDS. In Section 3, we present our results for a sample of 206 long bursts and investigate various correlations between the extracted parameters. In addition, we propose a new frequency–luminosity relation based on a sample of 58 GRBs with spectroscopically measured redshifts. In Section 4, we discuss observational biases of our results. Finally, in Section 5, we summarize our conclusions. In this work, we have adopted the standard values for the cosmological parameters: $\Omega_{\rm M} = 0.27, \Omega_{\rm L} = 0.73$ and the Hubble constant H_0 is 70 (km s^{-1}) Mpc^{-1}. Throughout this paper, the quoted uncertainties are at the 68 per cent confidence level, unless noted otherwise.

2 DATA ANALYSIS

2.1 Light-curve extraction

Swift Burst Alert Telescope (BAT) is a highly sensitive, coded aperture instrument (Barthelmy et al. 2005). BAT uses the shadow pattern resulting from the coded mask to facilitate few arcminute localization of gamma-ray sources. In order to generate background-subtracted LCs, we used a process called mask weighting. The mask weighting assigns a ray-traced shadow value for each individual event, which then enables the user to calculate LCs or spectra.

We used the batmaskwtevt and batbinevt tasks in the *Swift* BAT FTOOLS to generate mask-weighted, background-subtracted LCs in the BAT energy range of 15–200 keV. The LCs that are generated have rates that are measured in counts per second per detector (count s^{-1} det^{-1}). In addition, the above tools also generate uncertainties associated with the rates that are calculated by propagation of errors from raw counts (subject to Poissonian noise). For the BAT instrument, one can potentially go down to the minimum time binning of ∼0.1 ms. However, in this work, we used 1-ms time-binned LCs.

2.2 Fourier analysis

We calculate the Fourier transform, $a_{\rm f}$, of each GRB LC, $R(t)$ (measured in count s^{-1} det^{-1}), using a standard fast Fourier transform (FFT)[1] algorithm (Jenkins & Watts 1969; Press et al. 2002). We used a time segment of the burst LC where the total fluence is accumulated (i.e. start and end times corresponding to burst T100 which is calculated by the battblocks task). The PDS of each burst is calculated using $P_{\rm f} = a_{\rm f}\, a_{\rm f}^{*}$. The power spectra are not normalized nor are they averaged. In addition, we have employed logarithmic binning for our power spectra.

This process of treating PDS individually is different from that of Beloborodov et al. (1998, 2000), Lazzati (2002) and Borgonovo et al. (2007), as they used some averaging process to obtain the slope of the red-noise component of the power spectra. The wide variety of LCs exhibited by GRBs is potentially indicative of different emission and scattering processes that eventually shape the observed LCs, and therefore we have avoided averaging power spectra so as not to compromise this valuable information.

The uncertainties of the individual PDS are calculated as follows. For each burst, we simulate 100 LCs based on the original LC ($R_{\rm bin}^{\rm real}$) and its uncertainty ($R_{\rm bin}^{\rm real\ error}$), i.e.

$$R_{\rm bin}^{\rm simulated} = R_{\rm bin}^{\rm real} + \zeta \times R_{\rm bin}^{\rm real\ error}. \quad (1)$$

[1] We used the FFT routine in the Interactive Data Language (IDL) data analysis package. http://www.ittvis.com/ProductServices/IDL.aspx

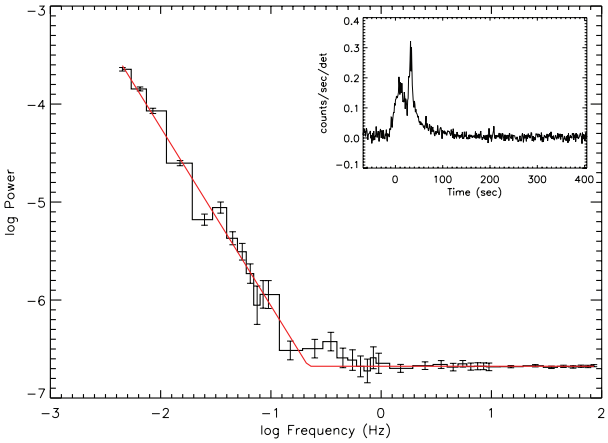

Figure 1. PDS of GRB 081203A. The low-frequency power-law component is referred to as the 'red-noise' component and the flat high-frequency region is called the 'white-noise' component. The inset shows the LC of GRB 081203A.

Here ζ is a random number generated from a Gaussian distribution with the mean equal to zero and the standard deviation equal to 1. For each simulated LC, we calculate a PDS. Then we rebin each PDS logarithmically. The uncertainties in the original PDS (obtained from the original LC) are derived by taking the standard deviation of the 100 simulated PDS.

The power spectra for the GRBs in the sample are fitted with the function depicted in equation (2) (see Fig. 1 for a typical fit). This function consists of a power-law component (to fit the low-frequency 'red-noise' component) and a constant component (to fit the flat high-frequency 'white-noise' component):

$$\log P(f) = \begin{cases} \alpha(\log f - \log f_{\rm th}) + \log P_{\rm w} & \text{for } f \le f_{\rm th} \\ \log P_{\rm w} & \text{for } f > f_{\rm th}. \end{cases} \quad (2)$$

Here $f_{\rm th}$ is the threshold frequency where the red-noise component intersects the white-noise component of the PDS and $P_{\rm w}$ is the white-noise power density.

3 RESULTS

Out of 451 GRBs which triggered *Swift* BAT from 2004 December 19 to 2009 December 31, we selected a sample of 226 long GRBs that show a significant red-noise component above the flat white-noise region. In Fig. 2, we represent the two samples (the sample with a clear red-noise component is shown in red boxes and the sample with no or weak red-noise component is shown in blue inverted triangles) in a peak-photon-flux versus T100-duration plot. For the most part, the bursts that do not show a clear red-noise component are generally either weak or short in duration.

For the selected sample of 226 long GRBs, we fitted the corresponding PDS with a simple power-law behaviour given in equation (2), using the non-linear least squares routine MPFIT (Markwardt 2009). A typical fit is shown in Fig. 1. Out of the 226 GRBs in the sample, 20 bursts could not be fitted by a simple power law. These GRBs were excluded from further analysis. For the final sample of 206 bursts, the distributions of the extracted slopes (α) and threshold frequencies ($f_{\rm th}$) are shown in Figs 3 and 4, respectively. The distribution in Fig. 3 has a Gaussian-like shape and peaks around ∼−1.4 with σ of about 0.6. The distribution of threshold frequencies in Fig. 4 peaks around 1 Hz and also shows a broad distribution. The distribution of the redshift-corrected $f_{\rm th}$ [i.e. $f_{\rm th}(1+z)$], as depicted

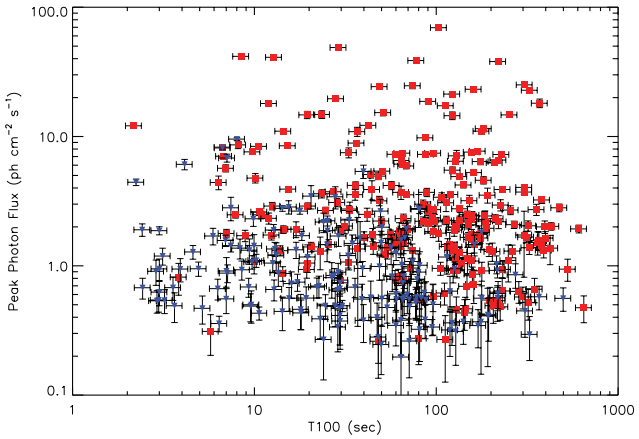

Figure 2. The peak photon flux versus the T100 duration. The final sample with a significant red-noise component is shown in red boxes and the sample with no or weak red-noise component is shown in blue inverted triangles. Note that conservative 10 per cent uncertainties were assumed for T100 values.

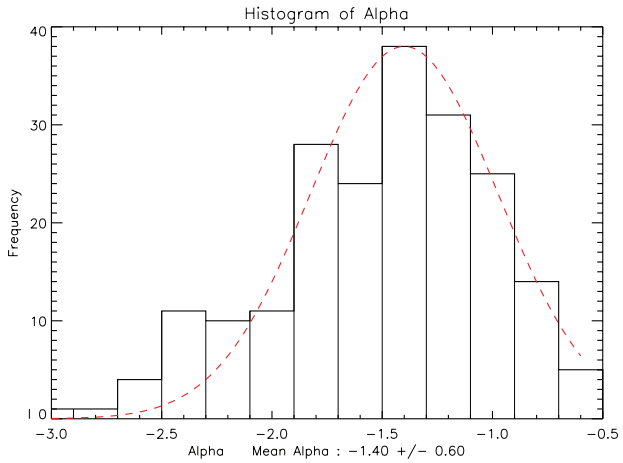

Figure 3. Histogram of the extracted slopes (α). The distribution shows a peak around -1.4 ± 0.6.

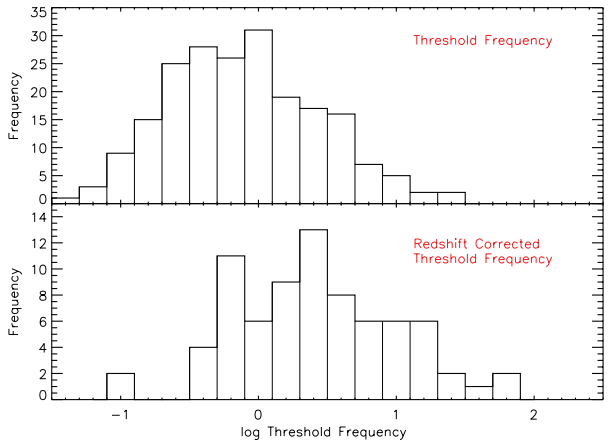

Figure 4. A histogram of extracted threshold frequencies ($f_{\rm th}$) is shown in the top panel. The histogram peaks around ∼1 Hz. The bottom panel shows a histogram of redshift-corrected $f_{\rm th}$ for the subset of bursts with redshift measurements. Both distributions show a large dispersion.

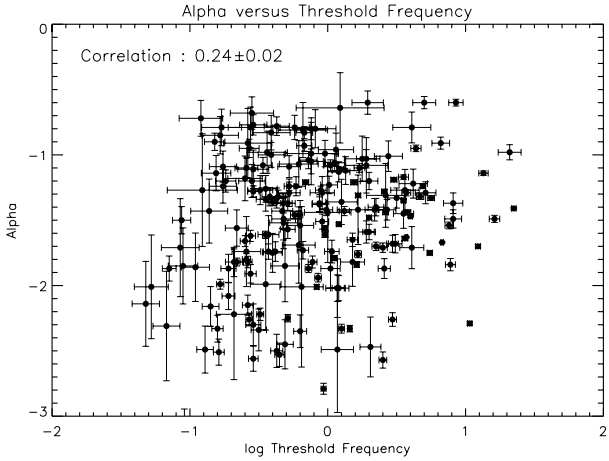

Figure 5. The extracted slope, α, as a function of the threshold frequency, $f_{\rm th}$. A very weak positive correlation is observed.

in the bottom panel of Fig. 4, shows a large dispersion and non-Gaussian shape. In Fig. 5, we show a plot of α and $f_{\rm th}$; we see a very weak positive correlation (0.24 ± 0.02) but we note at this stage of the analysis that $f_{\rm th}$ has not been corrected for noise contamination nor has it been corrected for redshift.

There are 76 GRBs in our sample with measured redshifts (spectroscopic or otherwise). For this sub-sample, it is interesting to see whether the extracted parameters are redshift dependent. Fig. 6 shows α (top panel), $f_{\rm th}$ (middle panel) and the redshift-corrected $f_{\rm th}$ (bottom panel) as a function of redshift. Very weak correlations are observed between α and redshift and also between $f_{\rm th}$ and redshift. However, no significant correlation is observed between $f_{\rm th}(1 + z)$ and redshift.

In Ukwatta et al. (2009), we proposed a correlation between the isotropic peak luminosity and the redshift-corrected $f_{\rm th}$ based on 27 GRBs. To investigate this further with a larger sample, we have selected a sample of 58 bursts with spectroscopically measured redshifts and good spectral information. For this sample, we have calculated isotropic peak luminosity as described in Ukwatta et al. (2010). Based on the availability of spectral information, we have divided the sample into three sub-samples: 'Gold', 'Silver' and 'Bronze'. The 'Gold' sample with 15 bursts have all Band spectral parameters measured (Band et al. 1993). In the 'Silver' sample (15 bursts), the $E_{\rm p}$ has been determined by fitting a cut-off power law[2] to spectra. These 15 bursts do not have the high-energy spectral index, β, measured, so we used the mean value of the BATSE β distribution, which is -2.36 ± 0.31 (Kaneko et al. 2006; Sakamoto et al. 2009). The 'Bronze' sample, with 28 bursts, does not have a measured $E_{\rm p}$. We have estimated it using the power-law index (Γ) of a simple power-law fit as described in Sakamoto et al. (2009). For these 28 bursts, the low-energy spectral index, α, and the high-energy spectral index, β, were not known, so we used the mean values of the BATSE α and β distributions, which are -0.87 ± 0.33 and -2.36 ± 0.31, respectively (Kaneko et al. 2006; Sakamoto et al. 2009).

The isotropic luminosity as a function of the redshift-corrected threshold frequency is shown in Fig. 7. In the figure, the 'Gold', 'Silver' and 'Bronze' samples are shown in red, blue and green filled circles, respectively. A clear positive correlation can be seen in the figure. The Pearson correlation coefficient is 0.77 ± 0.02, where the

[2] d N/d $E \sim E^{\alpha}$ exp [$-(2+\alpha)E/E_{\rm p}$].

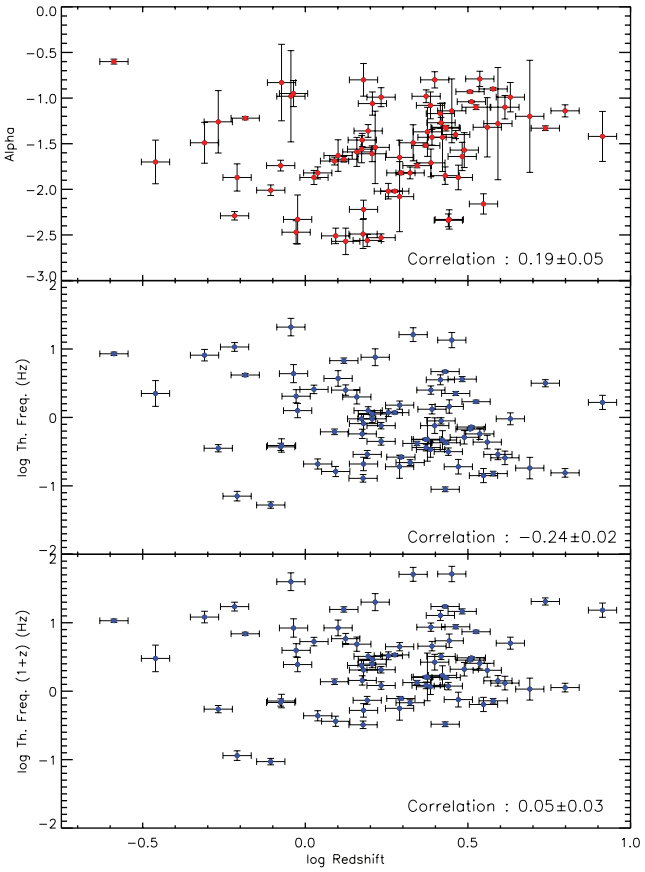

Figure 6. The slope α (top panel), the threshold frequency (middle panel) and redshift-corrected $f_{\rm th}$ (bottom panel) as a function of redshift. The top and the middle panels show very weak correlations while the bottom panel shows no significant correlation. Note that conservative 10 per cent uncertainties were assumed for redshift values.

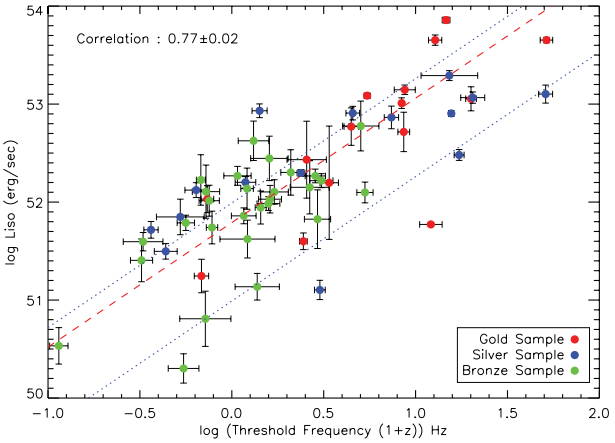

Figure 7. Isotropic peak luminosity as a function of the redshift- corrected threshold frequency, $f_{\rm th}(1+z)$. The parameters are correlated with a correlation coefficient of 0.77 ± 0.02 and the best-fitting power law yields an exponent of 1.27 ± 0.12.

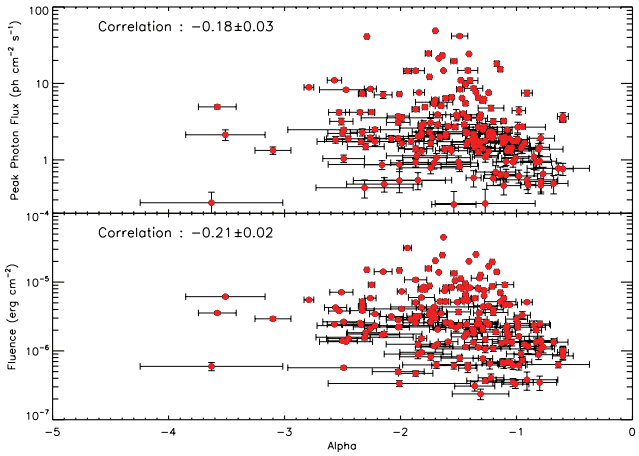

Figure 8. The peak photon flux (top panel) and the fluence (bottom panel) as a function of α. Very weak negative correlations are observed in both cases.

uncertainty was obtained through a Monte Carlo simulation. The probability that the above correlation occurs due to random chance is $\sim 4.5 \times 10^{-9}$. Our best fit is shown as a red dashed line in Fig. 7 yielding the following relation between $L_{\rm iso}$ and $f_{\rm th}$:

$$\log L_{\rm iso} = (51.79 \pm 0.12) + (1.27 \pm 0.12) \log[f_{\rm th}(z+1)]. \quad (3)$$

To compensate for the large scatter in the plot, the uncertainties of the fit parameters are multiplied by a factor of $\sqrt{\chi^2/{\rm ndf}} = \sqrt{1766/56} \approx 6.0$, where ndf is the number of degrees of freedom. The blue dotted lines indicate the estimated 1σ confidence level, which is obtained from the cumulative fraction of the residual distribution taken from 16 to 84 per cent.

Our result for the slope in Fig. 7 is consistent with the value of 1.4 ± 0.2 obtained by Ukwatta et al. (2009) using 27 GRBs. This is encouraging because the results of Ukwatta et al. (2009) were obtained using non-mask-weighted event-by-event data instead of the mask-weighted data that we use in the current work. We also note that with the increase in the sample size by about a factor of 2, the correlation coefficient has increased from 0.69 ± 0.03 to 0.77 ± 0.02. The correlation between frequency and luminosity is clearly intriguing but there remain observational biases which we address in a later section.

It has been reported previously (Beloborodov et al. 2000) that the PDS slope is correlated with the burst brightness. In order to check our sample for this effect, we display in Fig. 8 the slope (α) against brightness indicators: the peak photon flux and the fluence. Very weak negative correlations are observed in both cases.

The other extracted parameter, the noise crossing threshold frequency ($f_{\rm th}$) of the PDS, is also expected to depend on the brightness of the GRB. Presumably, the 'red-noise' component of the PDS comes primarily from the GRB but the flat 'white-noise' component can in principle arise from the Poisson noise (intensity fluctuations) associated with the GRB and the natural background in the field of view of the detector. For distant and/or intrinsically weak bursts, noise unrelated to the burst may dominate the observed white-noise component, thereby overwhelming the red-noise part of the signal. This, in turn, would make the extraction of the threshold frequency brightness-dependent. In Fig. 9, we plot the peak photon flux and the photon fluence as a function of the threshold frequency. The red dashed line in the top panel of Fig. 9 is the best fit, given by equation (4), and blue dotted lines indicate a 1σ confidence interval:

$$\log {\rm PPF} = (0.58 \pm 0.03) + (0.82 \pm 0.04) \log f_{\rm th}. \quad (4)$$

Indeed, a positive correlation can be seen between $f_{\rm th}$ and the peak photon flux. However, no significant correlation is observed between $f_{\rm th}$ and fluence. We discuss this important matter further in the next section.

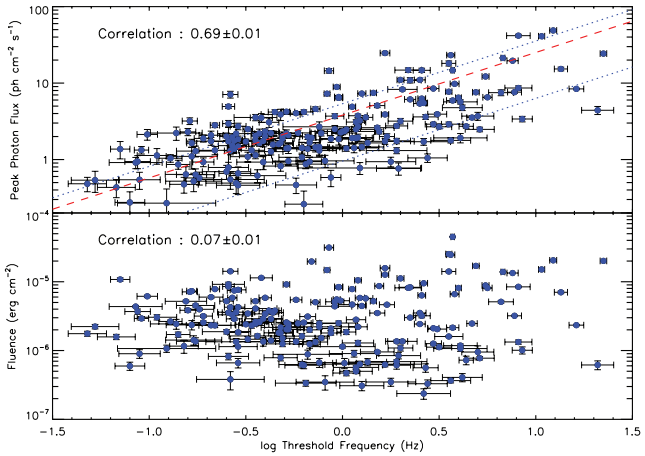

Figure 9. The peak photon flux as a function of threshold frequency (top panel) and the photon fluence as a function of threshold frequency (bottom panel). No significant correlation is observed between fluence and $f_{\rm th}$ but a significant correlation is observed between peak photon flux and $f_{\rm th}$.

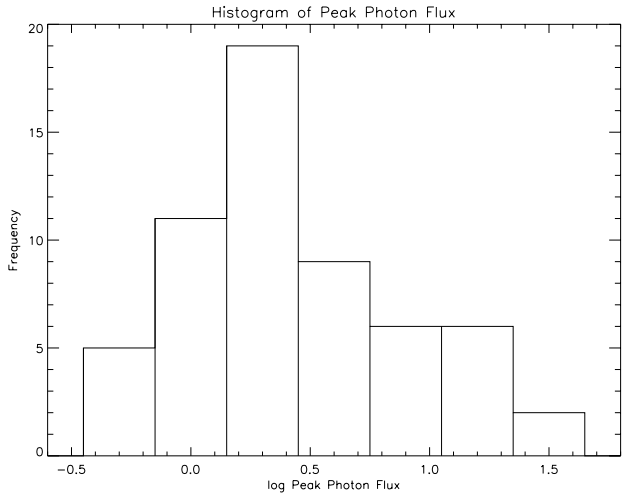

Figure 10. Histogram of the peak photon flux of the sample of 58 bursts used to generate Fig. 7.

4 DISCUSSION

It is conceivable that the proposed frequency–luminosity correlation is a direct result of the observed correlation between $f_{\rm th}$ and the peak photon flux of the burst (see the top panel of Fig. 9). If this is the case, then for a statistically significant sample of bursts with similar apparent brightness, we should not see a correlation between $f_{\rm th}$ and $L_{\rm iso}$. In order to select a sample of GRBs with similar apparent brightness, we plot in Fig. 10 the peak photon flux distribution for the sample of 58 bursts used to investigate the frequency–luminosity correlation in Fig. 7. We see from Fig. 10 that about half of the sample (28 GRBs) have a very similar peak photon flux [$0.0 < \log$ (peak photon flux) < 0.5]. For this subset of bursts, we plotted their peak photon flux and $L_{\rm iso}$ as a function of $f_{\rm th}$ and the results are shown in Fig. 11. In the top panel of Fig. 11, it is clear that there is a significant correlation between $f_{\rm th}$ and $L_{\rm iso}$ with a correlation coefficient of 0.60 ± 0.06. This implies that the correlation observed in Fig. 7 [$f_{\rm th}(1+z)$–$L_{\rm iso}$ correlation] is not entirely due to the correlation seen in the top panel of Fig. 9 ($f_{\rm th}$–peak-photon-flux correlation). We now correct the $f_{\rm th}$ of this limited sample (with similar apparent brightness) for redshift to see its effect. Plotted in

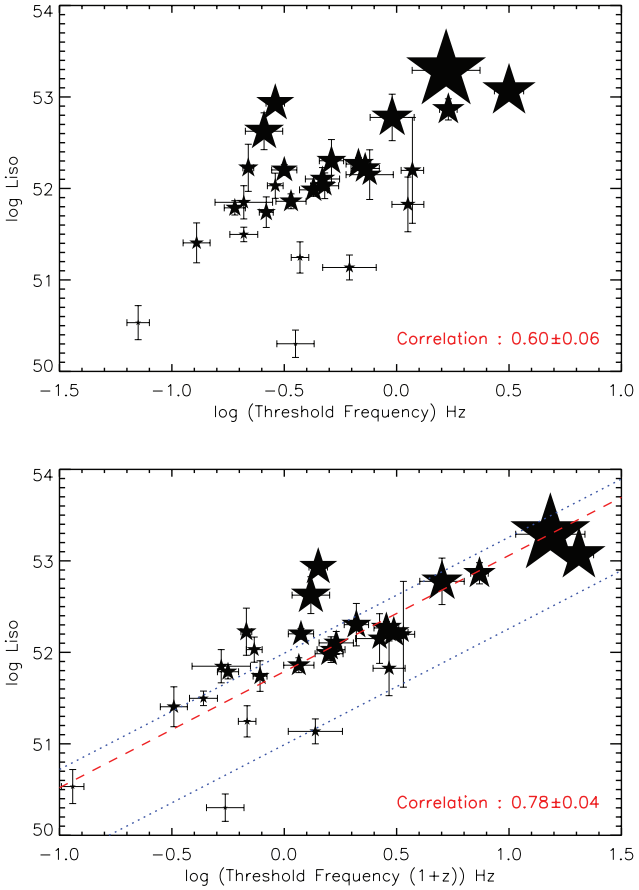

Figure 11. The isotropic peak luminosity as a function of threshold frequency (with and without redshift correction) for a sample of bursts with a narrow apparent brightness range. The red dashed and blue dotted lines are the same fit curves as shown in Fig. 7. The size of the star is proportional to the redshift of the burst.

the bottom panel of Fig. 11 are the redshift-corrected data. We note that the correlation strength increases to a value of 0.78 ± 0.04, in part due to the natural correlation between redshift and $L_{\rm iso}$.

In addition, we can approach the issue from the other direction, i.e. we select a subset of bursts with similar luminosity and ask the question whether the correlation between the peak photon flux and $f_{\rm th}$ comes from the proposed $f_{\rm th}(1+z)$–$L_{\rm iso}$ correlation. In order to perform this test, we selected a subset of bursts which have roughly the same $L_{\rm iso}$ values ($51.5 < \log L_{\rm iso} < 52.5$) and plotted their peak photon flux as a function of $f_{\rm th}$. In Fig. 12, we show the peak photon flux as a function of $f_{\rm th}$ (top panel) and the redshift-corrected $f_{\rm th}$ (bottom panel). There is clearly a strong correlation between the two parameters in both panels. It is interesting, however, that after the redshift correction, the correlation strength drops significantly. Accordingly, it would appear that the correlation between the peak photon flux and $f_{\rm th}$ (top panel of Fig. 9) is not entirely due to the $f_{\rm th}(1+z)$–$L_{\rm iso}$ correlation (Fig. 7). Since the spectral power is proportional to the square of the flux and the PDS follows an $f^{-\alpha}$ behaviour (see Fig. 3), we expect to see a correlation between the peak photon flux and $f_{\rm th}$. Hence, this correlation is in most part observational.

Now we turn to the question of the dependence of the extracted threshold frequency on the noise level (NL) of the burst. The obvious question is how to determine the NL for each burst. One way of

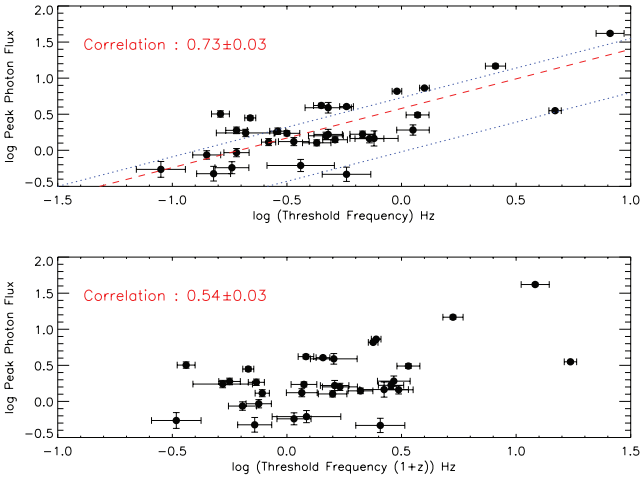

Figure 12. Peak photon flux as a function of $f_{\rm th}$ (top panel) and redshift-corrected $f_{\rm th}$ (bottom panel) for a sample bursts with roughly constant luminosity. The red dashed line in the top panel is the best-fitting line obtained in Fig. 9 and the blue dotted lines indicate the 1σ confidence interval.

defining the NL is as follows:

$$\text{Noise level} = \frac{\text{Std. dev. (detrended LC)}}{\text{Peak count rate}} \times 100 \text{ per cent.} \quad (5)$$

The detrending of the LC can be done in a number of ways and we adopted the following method. We generated two LCs of the same burst with two bin sizes. In order to produce the coarser binned LC, we chose a time bin size that resulted in at least 100 points in the burst duration (T100). The other LC may have bin sizes that vary from 1 ms up to the coarser bin size. Clearly, with the different binning, the two LCs will have a different number of points. In order to properly detrend, we need to have the same number of points in the two LCs. We accomplish this by using a simple linear interpolation of the coarser binned LC. The interpolated LC is then subtracted from the finer binned LC to generate the detrended LC.

Using equation (5), we extract an NL for each burst. However, the extracted NL depends on the bin size used in the detrending process. This aspect needs to be either removed or accounted for before the NL of all the bursts can be treated on an equal footing.

The level of the flat white-noise region of the PDS does not depend on the bin size, i.e. for a given burst the white NL is constant irrespective of the bin size, and for that matter so too are the extracted parameters α and $f_{\rm th}$. In order to remove the bin size dependence in the extraction of the NL, we modify equation (5) as follows:

$$\text{Noise level} = \frac{1}{\sqrt{N}} \frac{\text{Std. dev. (detrended LC)}}{\text{Peak count rate}} \times 100 \text{ per cent.} \quad (6)$$

Here N is the number of data points in the finely binned LC. Our tests indicate that the results given by equation (6) do not depend on the time bin size of the LC and provide a robust measure of the NL of a given burst.

In order to further investigate the dependence of $f_{\rm th}$ on the NL, we performed additional tests. We simulated different NLs by adding increasing amounts of Gaussian noise to a burst LC (in this case GRB 050315). Then we extracted $f_{\rm th}$ values for each setting of the NL. Our results, the extracted frequency values versus the NL, are shown in Fig. 13 as a log–log plot. The threshold frequency does indeed depend on the NL. However, there is a linear relationship between the logarithmic values of the two quantities. This relation is important to know because it can be used to correct the extracted

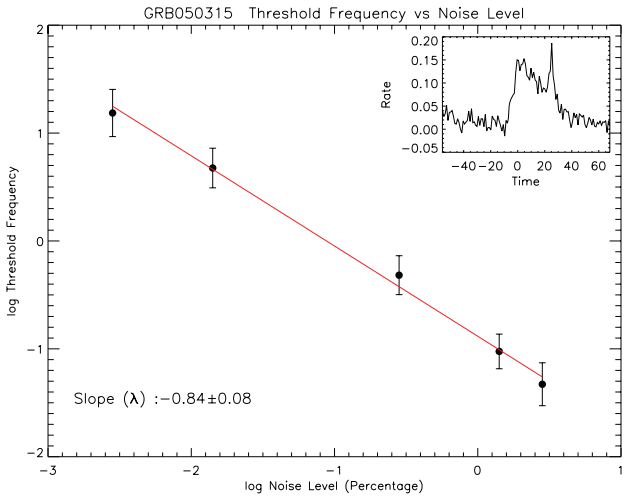

Figure 13. The extracted threshold frequency as a function of the NL in a log–log scale. The threshold frequency displays a power-law dependence on the NL of the burst with an index (λ) of -0.84 ± 0.08 for GRB 050315. The inset shows the time profile of the burst.

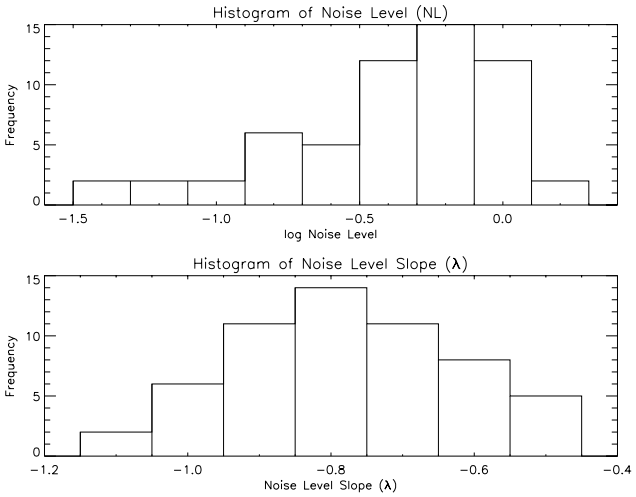

Figure 14. Distribution of NLs (top panel) and NL slope, λ (bottom panel) in the sample.

$f_{\rm th}$ values to some nominal NL that is common to all bursts in the sample.

By performing the same test on the other bursts in our sample, we established that the relation between $f_{\rm th}$ and the NL depends on the profile of the burst, i.e. the slope (λ) of the log–log plot is different for each burst. Shown in the bottom panel of Fig. 14 is the distribution of the slopes, λ, obtained for our sample of 58 bursts used in the $f_{\rm th}$–$L_{\rm iso}$ relation. Correspondingly, the NL distribution is shown in the top panel of Fig. 14. This distribution shows a clear peak around the log value of -0.2 (NL $\sim$ 0.6) while the λ distribution peaks around the value of -0.8.

We are now in a position to treat all the bursts in our sample on an equal footing and test whether the $f_{\rm th}$–$L_{\rm iso}$ correlation, observed in Fig. 7, survives. The aim is to extract threshold frequencies which are consistent with an NL that is common to all the bursts in our sample. In order to accomplish this, we choose an arbitrary NL of 1.0 (see Fig. 13) and use the following relation to extract a corrected $f_{\rm th}$ for each burst:

$$\log f_{\rm th[NL=1]} = \log f_{\rm th[NL=burst]} - \lambda_{\rm burst} \log(\rm NL_{[NL=burst]}). \quad (7)$$

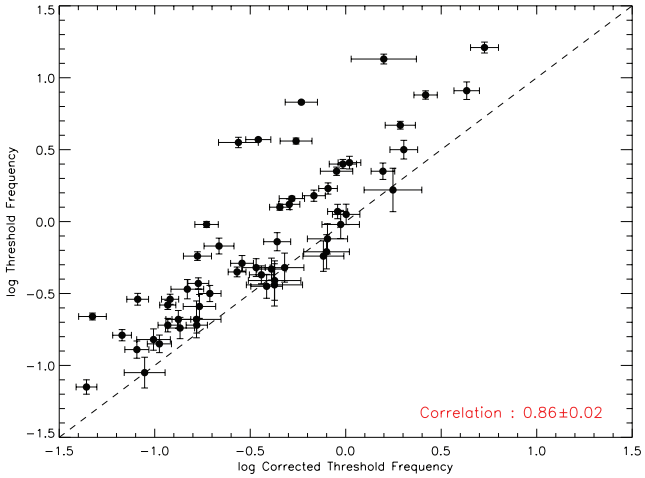

Figure 15. The threshold frequency versus the noise-corrected threshold frequency. The two parameters show a strong correlation with a correlation coefficient of 0.86. The dashed line indicates the equality line of the two parameters.

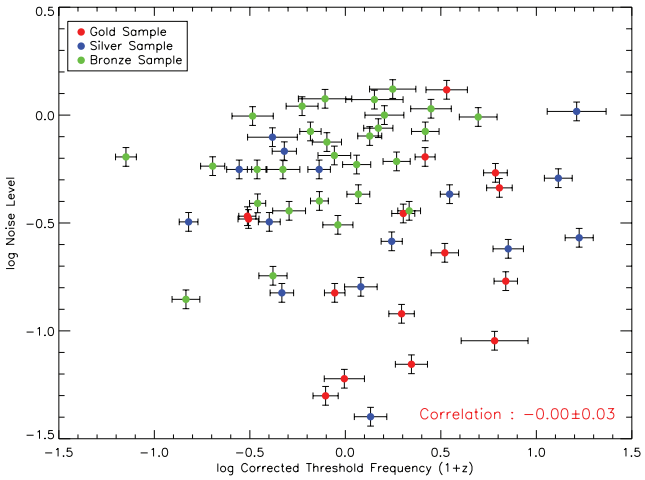

Figure 16. The noise-corrected, redshift-corrected threshold frequency versus NL.

Here, $f_{\mathrm{th[NL=burst]}}$ is the extracted threshold frequency for a given burst, λ_{burst} is the NL slope corresponding to the same burst and $\mathrm{NL}_{\mathrm{[NL=burst]}}$ is the burst NL determined by equation (6). The correction procedure is repeated for each burst in our sample. To gauge the size of the correction, we plot in Fig. 15 (in a log–log scale) the corrected f_{th} values versus the uncorrected f_{th}. We note that there is a strong correlation between the two parameters. This is a reflection of the clustering of the NL and λ seen in Fig. 14. We also plotted the NL as a function of the noise-corrected, redshift-corrected f_{th} in Fig. 16. There is no correlation between these two parameters, thus giving us confidence in the noise correction procedure.

We show in Fig. 17 the noise-corrected threshold frequency–luminosity relation. As is evident, the relation survives the noise correction albeit with a somewhat smaller correlation coefficient of 0.57 ± 0.03. Various correlation coefficients of the relation are shown in Table 1, where the uncertainties were obtained through a Monte Carlo simulation. The null probability that the correlation occurs due to random chance is also given for each coefficient type.

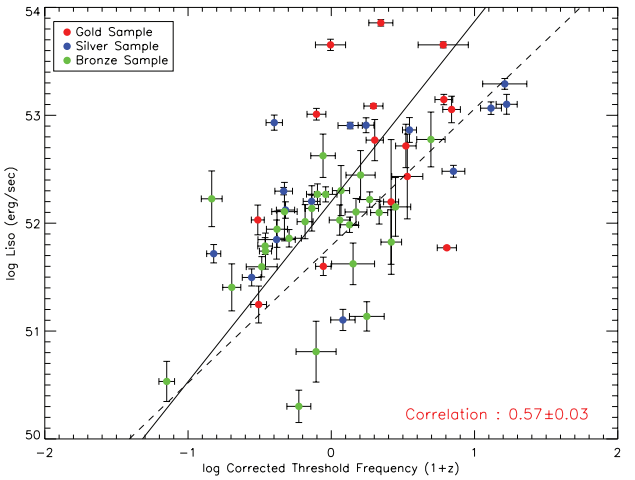

Figure 17. The noise-corrected, redshift-corrected threshold frequency versus isotropic peak luminosity. The correlation coefficient between the two parameters is 0.57 ± 0.03. The solid line shows the best-fitting power law with an index of 1.67 ± 0.01. The dashed line shows the best fit from Fig. 7.

Table 1. Correlation coefficients.

Coefficient type	Correlation coefficient	Null probability
Pearson's r	0.57±0.03	1.42×10^{-5}
Spearman's r_s	0.58±0.04	1.72×10^{-6}
Kendall's τ	0.43±0.03	2.03×10^{-6}

The new best fit is shown as a solid line in Fig. 17 yielding the following relation between L_{iso} and $f_{\mathrm{th[NL=1]}}$:

$$\log L_{\mathrm{iso}} = (52.2 \pm 0.1) + (1.67 \pm 0.01) \log[f_{\mathrm{th}}(z+1)]. \quad (8)$$

The uncertainties in the fitted parameters are expressed with the factor of $\sqrt{\chi^2/\mathrm{ndf}} = \sqrt{1255/56} \approx 5.0$.

5 CONCLUSION

In this paper, we have analysed PDS of 206 GRBs. We fitted each PDS with a simple power law and determined the red-noise exponent and the threshold frequency where white noise begins. For a subset of GRBs, we extracted a frequency–luminosity relationship. For this sample, we treated all bursts on an equal footing by determining a common NL, thereby minimizing the potential observational biases. We summarize the main results of our analysis as follows.

(i) The distribution of the extracted α (slope of the red-noise component) values peaks around -1.4 and that of f_{th} around 1 Hz.

(ii) The dispersion in the distribution of α is large and so the Kolmogorov index of $-5/3$ is accommodated by our analysis.

(iii) The distribution of the redshift-corrected threshold frequency shows a large dispersion and is non-Gaussian in shape.

(iv) Evidence is presented for a possible frequency–luminosity relationship, i.e. the redshift-corrected f_{th} is correlated with the isotropic luminosity. The correlation coefficient is 0.57 ± 0.03 and the best-fitting power law has an index of 1.67 ± 0.01. We appreciate that in reality there may be complicated underlying interrelationships involving peak photon flux, f_{th}, and redshift and therefore the evidence for the frequency–luminosity relation should be considered tentative.

(v) The proposed frequency–luminosity correlation, if confirmed, may serve to provide a measure of the intrinsic variability observed in GRBs.

ACKNOWLEDGMENTS

We thank the anonymous referee for comments and suggestions that significantly improved the paper. We also thank T. Sakamoto and C. Guidorzi for useful discussions. The NASA grant NNX08AR44A provided partial support for this work and is gratefully acknowledged.

REFERENCES

Band D. et al., 1993, ApJ, 413, 281
Barthelmy S. D. et al., 2005, Space Sci. Rev., 120, 143
Beloborodov A. M., Stern B. E., Svensson R., 1998, ApJ, 508, L25
Beloborodov A. M., Stern B. E., Svensson R., 2000, ApJ, 535, 158
Borgonovo L., Frontera F., Guidorzi C., Montanari E., Vetere L., Soffitta P., 2007, A&A, 465, 765
Fenimore E. E., Ramirez-Ruiz E., 2000, preprint (arXiv:astro-ph/0004176)
Gehrels N. et al., 2004, ApJ, 611, 1005
Giblin T. W., Kouveliotou C., van Paradijs J., 1998, in Meegan C. A., Preece R. D., Koshut T. M., eds, 4th Hunstville Symp. Vol. 428, Power Spectra of BATSE GRB Time Profiles, Gamma-Ray Bursts. Am. Inst. Phys., New York, p. 241
Guidorzi C., 2005, MNRAS, 364, 163
Guidorzi C., Frontera F., Montanari E., Rossi F., Amati L., Gomboc A., Hurley K., Mundell C. G., 2005, MNRAS, 363, 315
Guidorzi C., Frontera F., Montanari E., Rossi F., Amati L., Gomboc A., Mundell C. G., 2006, MNRAS, 371, 843
Jenkins G. M., Watts D. G., 1969, Holden-Day Series in Time Series Analysis. Holden-Day, London
Kaneko Y., Preece R. D., Briggs M. S., Paciesas W. S., Meegan C. A., Band D. L., 2006, ApJS, 166, 298
Lazzati D., 2002, MNRAS, 337, 1426
Li L.-X., Paczyński B., 2006, MNRAS, 366, 219
Markwardt C. B., 2009, in Bohlender D. A., Durand D., Dowler P., eds, ASP Conf. Ser. Vol. 411, Astronomical Data Analysis Software and Systems XVIII. Astron. Soc. Pac., San Francisco, p. 251
Press W. H., Teukolsky S. A., Vetterling W. T., Flannery B. P., 2002, Numerical Recipes in C++: The Art of Scientific Computing. Cambridge Univ. Press, Cambridge
Reichart D. E., Lamb D. Q., Fenimore E. E., Ramirez-Ruiz E., Cline T. L., Hurley K., 2001, ApJ, 552, 57
Rizzuto D. et al., 2007, MNRAS, 379, 619
Sakamoto T. et al., 2009, ApJ, 693, 922
Ukwatta T. N. et al., 2009, preprint (arXiv:0906.3193)
Ukwatta T. N. et al., 2010, ApJ, 711, 1073

This paper has been typeset from a TEX/LATEX file prepared by the author.